



**HAL**  
open science

# Monte Carlo Simulation of Atmospheric Radiative Forcings Using A Path-Integral Formulation Approach for Spectro-Radiative Sensitivities

Mourtaday Nada, Bati Mégane, Blanco Stéphane, Dufresne Jean-Louis, Mouna El-Hafi, Eymet Vincent, Forest Vincent, Fournier Richard, Gautrais Jacques, Lapeyre Paule, et al.

► **To cite this version:**

Mourtaday Nada, Bati Mégane, Blanco Stéphane, Dufresne Jean-Louis, Mouna El-Hafi, et al.. Monte Carlo Simulation of Atmospheric Radiative Forcings Using A Path-Integral Formulation Approach for Spectro-Radiative Sensitivities. 2024. hal-04432801v1

**HAL Id: hal-04432801**

**<https://hal.science/hal-04432801v1>**

Preprint submitted on 1 Feb 2024 (v1), last revised 26 Aug 2024 (v2)

**HAL** is a multi-disciplinary open access archive for the deposit and dissemination of scientific research documents, whether they are published or not. The documents may come from teaching and research institutions in France or abroad, or from public or private research centers.

L'archive ouverte pluridisciplinaire **HAL**, est destinée au dépôt et à la diffusion de documents scientifiques de niveau recherche, publiés ou non, émanant des établissements d'enseignement et de recherche français ou étrangers, des laboratoires publics ou privés.

# Monte Carlo Simulation of Atmospheric Radiative Forcings Using A Path-Integral Formulation Approach for Spectro-Radiative Sensitivities

Mourtaday Nada<sup>1\*</sup>, Bati Mégane<sup>1</sup>, Blanco Stéphane<sup>1</sup>, Dufresne Jean-Louis<sup>2</sup>, El Hafi Mouna<sup>1,3</sup>, Eymet Vincent<sup>4</sup>, Forest Vincent<sup>4</sup>, Fournier Richard<sup>1</sup>, Gautrais Jacques<sup>5,1</sup>, Lapeyre Paule<sup>6</sup>, Nyffenegger-Péré Yaniss<sup>1</sup>, Villefranque Najda<sup>7</sup>.

**1** LAPLACE, Université de Toulouse, CNRS, INPT, UPS, Toulouse, France.

**2** LMD/IPSL, Sorbonne Université, CNRS, École Polytechnique, ENS, Paris, France.

**3** Université de Toulouse, Mines Albi, UMR 5302 - Centre RAPSODEE, Campus Jarlard, F-81013, Albi CT cedex 09, France.

**4** Méso-Star, Toulouse, France.

**5** CRCA, CBI, Université de Toulouse, CNRS, Toulouse, France.

**6** Department of Mechanical and Mechatronics Engineering, University of Waterloo, 200 University Ave. W, Waterloo ON, Canada

**7** Centre National de Recherches Météorologiques, UMR 3589 CNRS, Météo France, Toulouse, France.

\* corresponding author: mourtadaynadachems@gmail.com

## Abstract

We present recent advances in path-integral formulations designed for unbiased Monte Carlo sensitivity estimation (in the form of partial derivatives) within a coupled physics model. We establish the theoretical foundation and illustrate the approach by estimating instantaneous atmospheric radiative forcings. In climate studies, these quantities amount for the change in top-of-atmosphere (TOA) net radiative flux induced by an isolated change in surface or atmospheric constitution. Based on a path-integral framework, our approach results in estimations consistent with well-established radiative forcings in the climate community. We highlight how physics coupling through path-integral formulations yields unbiased sensitivity estimation of a radiative quantity (integrated TOA flux) to a spectroscopic parameter (fraction change in gas concentration). Furthermore, we emphasize the method's scalability, demonstrating its compatibility with computer science acceleration techniques. These latter play a key role in rendering the computational time weakly sensitive to the system's multidimensional and multiphysics complexity.

## 1 Introduction and context

Monte Carlo methods yield unbiased estimates of integral quantities and their uncertainties, and as such, they have been employed for decades to provide reference results in atmospheric radiative transfer studies. Although being extensively used for benchmarking faster 1D radiative transfer codes to guide improvements in remote sensing, weather forecast and climate modeling, the high computational cost of Monte Carlo 3D codes, such as the I3RC community model [1] or MYSTIC [2], usually prevents their direct employment in operational contexts. However, recent transfer from computer science acceleration techniques to atmospheric radiative transfer science — to handle complex surfaces and detailed cloud fields for instance [3, 4, 5] — open new perspectives for using Monte Carlo methods beyond reference simulations. Indeed, these methods have recently been shown

to be key in addressing multiphysics and multidimensional integrals [6] resulting in computationally efficient simulations that are insensitive to the size and complexity of the integration domains [5, 7, 8].

A recent example in this respect is a novel work that couples a line-by-line spectroscopic model to a radiative transfer model, resulting in a spectro-radiative model first described in [9], that has recently benefited from a close collaboration between multiple communities (computer science, atmospheric science, spectroscopy and radiative transfer physics). This collaboration has resulted in a Monte Carlo radiative transfer code specifically designed to estimate integrated radiative fluxes. Developed during the PhD work of Nyffenegger-P  r   [16], it provides reference results for estimating atmospheric radiative fluxes integrated over any spatial, temporal and wavenumber domain, using the atmosphere and the surface properties’ description as input data, typically derived from a global and multi-decadal General Circulation Model (GCM) simulation. A concrete application of this tool in climate science is estimating the global broadband flux at TOA, that is, radiances averaged temporally over a climate period and spatially over the whole globe, as well as integrated over all frequencies and outgoing directions, without any compromise on the radiative or the spectroscopic physics description. Moreover, the approach combines path-integral Monte Carlo methods — insensitive to the integration domains — with computer graphics acceleration techniques [10, 11, 26] — that guarantee fast convergence —, resulting in computation times of just a few seconds that are insensitive to the input data complexity. Consequently, the computational cost for estimating the radiative flux integrated over an entire century, the entire globe, and the entire infrared spectrum is comparable to the cost for one particular time, location, and wavenumber, for the same precision level [16].

As the partial derivatives of an integral quantity are themselves integrals, initial developments for constructing path-integral sensitivities have been available for about 20 years [12], offering the benefit of providing uncertainties for these estimates. Since then, multiple studies [13, 17, 18, 19] have demonstrated that if we can estimate a quantity through Monte Carlo methods, then we also know how to estimate its sensitivities using these methods. However, statistical convergence issues often arise when estimating sensitivities in a manner specific to each application, making them at the heart of active fields of research, including computer graphics science [13]. Now, instantaneous radiative forcing — precisely the quantity we aim to estimate without bias from the perspective of the spectro-radiative model — can be determined in specific instances through sensitivity estimates, as illustrated in Section 3 for carbon dioxide concentrations. The instantaneous radiative forcing with respect to a parameter is defined as the variation in the outgoing radiative flux at TOA when this parameter value is changed while keeping the other physics model parameters fixed. Indeed, analyzing the physical mechanisms of global warming requires characterizing its evolution as a function of the climate system state. A first step is often to evaluate the radiative forcing resulting from a change in surface or atmospheric constitution (e.g., gas, cloud, aerosol, or surface properties), which are parameters in the spectro-radiative model. Instead of computing two estimates based on different sets of parameter values for a finite differences estimation, sensitivities can be estimated using the straightforward path-integral Monte Carlo methods that differentiate the spectro-radiative model. The unbiased nature of these estimations on both the modeling level (through the path-integral formulation for physics coupling) and the simulation level (through Monte Carlo methods) is crucial. Indeed, the presence of approximations in the treatment of radiative transfer or spectroscopic processes introduces disparities in the forcings computed by different climate models [22, 23]. Therefore, in the present work, we argue that in addition to estimating the radiative flux at TOA, we can build upon the spectro-radiative model framework to yield sensitivity estimates to any parameters of interest.

Section 2 serves as the theoretical framework of our approach, structured into three segments. In Section 2.1, we provide a succinct examination of the difficulties associated with calculating radiance. Next, we outline the path-integral foundations of its efficient Monte Carlo estimation through the null-collision technique [14]. Moving to Section 2.2, we establish a transport model for sensitivities that shares strong physical similarities with the transport of radiance. As a result, it is shown that the theoretical advancements presented for estimating radiance can also be applied to estimate sensitivities and thus radiative forcings. In Section 2.3, the Monte Carlo simulation algorithm associated with the resulting sensitivity path-integral is detailed. This lays the groundwork for an in-depth discussion of the sensitivity results in Section 3.

## 2 Theory and methods

### 2.1 Estimating global outgoing radiative flux at TOA

The global outgoing radiative flux at TOA,  $\bar{\phi}$ , is the monochromatic radiance  $L_\nu$  averaged over a time period  $\Delta t$  (typically 1 to 30 years), over the entire globe of area  $S$ , and integrated over all frequencies  $\nu$  and outgoing directions  $\vec{u}$ :

$$\bar{\phi} = \frac{1}{S\Delta t} \int_{\Delta t} dt \int_S dS(\vec{x}) \int_0^{+\infty} d\nu \int_{2\pi} d\vec{u} |\vec{u} \cdot \vec{n}| L_\nu(\vec{x}, \vec{u}, t) \quad (1)$$

That can easily be reformulated as the following path-integral:

$$\bar{\phi} = \int_{\Delta t} p_T(t) dt \int_S p_S(\vec{x}) dS(\vec{x}) \int_0^{+\infty} p_N(\nu) d\nu \int_{2\pi} p_U(\vec{u}) d\vec{u} \left\{ \frac{\pi L_\nu(\vec{x}, \vec{u}, t)}{p_N(\nu)} \right\} \quad (2)$$

Provided that functions  $p_T(t)$ ,  $p_S(\vec{x})$ ,  $p_N(\nu)$  and  $p_U(\vec{u})$  are normalized over their respective domains of definition, this path-integral can be formulated as the expectancy of a random variable  $\Omega$  defined over  $\cdot$ .  $\bar{\phi}$  can therefore be estimated using a Monte Carlo algorithm that uses the following probability density functions (PDFs) for sampling:

- $p_T(t) = 1/\Delta t$  is a uniform probability density function used to sample values of time  $t$  over the  $[t_0, t_0 + \Delta t]$  range,
- $p_S(\vec{x}) = 1/S$  is a uniform probability density function used to sample positions  $\vec{x}$  over the surface  $S$  of a sphere that represents the Earth's TOA,
- $p_N(\nu)$  is a probability density function used to sample values of frequency  $\nu$  over the  $[0, +\infty[$  range. Employing importance sampling to account for frequencies in proportion to their contributions, we choose a probability density function that follows the Planck function, expressed for the maximal temperature encountered in the system  $T_{max}$ . Since  $\int_0^{+\infty} L_\nu^{eq} d\nu = \sigma T_{max}^4 / \pi$ , we choose  $p_N(\nu) = (\pi L_\nu^{eq}) / \sigma T_{max}^4$ ,
- $p_U(\vec{u}) = |\vec{u} \cdot \vec{n}| / \pi$  is the probability density function used to sample an outgoing direction  $\vec{u}$  over the upper hemisphere following Lambertian emission.

Equation 2 unfolds as a linearly nested sequence of integrals over time, space, frequency, and direction. Consequently, using the *double randomization* principle [27, 28], a *single* Monte Carlo iteration for this multiple path-integral requires only a *single* sampling over *each* of the probability density functions. To break it down, one Monte Carlo realization of  $\bar{\phi}$  involves sequentially sampling a time  $t$  over  $[0, \Delta t]$  according to  $p_T(t)$ , a position  $\vec{x}$  over  $S$  according to  $p_S(\vec{x})$ , a frequency  $\nu$  over  $[0, +\infty[$  according to  $p_N(\nu)$  and a direction  $\vec{u}$  over the outgoing hemisphere at  $\vec{x}$  according to  $p_U(\vec{u})$ . The retained weight

of the realization is then  $\omega = \pi L_\nu(\vec{x}, \vec{u}, t)/p_N(\nu)$ , of variance  $\text{Var}(\omega)$ . According to the Central Limit Theorem, performing a large number of realizations  $N$ , their sample mean is a random variable  $\bar{\Omega}$  which follows a normal distribution of variance  $\text{Var}(\bar{\Omega}) = \text{Var}(\Omega)/N$ . As a realization of  $\bar{\Omega}$ , the sample mean  $\bar{\omega}$  of variance is an unbiased estimator for  $\bar{\phi}$ , for which  $\text{Var}(\omega)/(N-1)$  is an unbiased estimator for variance.

In practice, the monochromatic radiance field  $L_\nu(\vec{x}, \vec{u}, t)$  is unknown. If the expression for  $L_\nu$  within a heterogeneous and anisothermal participating medium can be formulated as a path integral formulation, easily implementable using Monte Carlo methods, then the double randomization technique can be extended over its integration domains. This extension entails sampling a single realization of its corresponding random variables. Our aim is the development of such a path-integral formulation.

The transport of radiance can be described by the stationary form of the monochromatic Radiative Transfer Equation (RTE):

$$\left\{ \begin{array}{l} \forall \vec{x} \in \Omega, \forall \vec{u} \in \mathbf{S}^2 : \\ \vec{u} \cdot \vec{\nabla} L_\nu(\vec{x}, \vec{u}) = -k_{\text{ext},\nu}(\vec{x}) L_\nu(\vec{x}, \vec{u}) + k_{a,\nu}(\vec{x}) L_\nu^{\text{eq}}(T(\vec{x})) \\ \quad + k_{s,\nu}(\vec{x}) \int_{4\pi} p_\nu(\vec{u}', \vec{u}) d\vec{u}' L_\nu(\vec{x}, \vec{u}') \\ \forall \vec{y} \in \partial\Omega, \forall \vec{u}_+ \in \mathbf{S}_+^2 : \\ L_\nu(\vec{y}, \vec{u}_+) = L_\nu^{\partial\Omega}(\vec{y}, \vec{u}_+) \end{array} \right. \quad (3)$$

where  $\mathbf{S}^2$  is the unit sphere,  $\Omega$  is the geometrical domain (the atmosphere), and  $\partial\Omega$  is its boundary (the TOA and the land or oceanic surface), where the monochromatic radiance  $L_\nu^{\partial\Omega}$  is known for all locations  $\vec{y} \in \partial\Omega$ , and all directions  $\vec{u}_+$  within the incoming hemisphere  $\mathbf{S}_+^2$  at position  $\vec{y}$ . The coefficients  $k_{a,\nu}(\vec{x})$ ,  $k_{s,\nu}(\vec{x})$ , and  $k_{\text{ext},\nu}(\vec{x}) = k_{a,\nu}(\vec{x}) + k_{s,\nu}(\vec{x})$  are the absorption, scattering, and extinction coefficients, respectively.  $L_\nu^{\text{eq}}(T(\vec{x}))$  is the equilibrium blackbody radiance (following the Planck blackbody radiance function, for temperature  $T(\vec{x})$  at location  $\vec{x}$ ), and  $p_\nu(\vec{u}', \vec{u})$  is the single scattering phase function, i.e., the probability density that the propagation direction after scattering is  $\vec{u}'$  for a given incoming direction  $\vec{u}$ .

The path-integral formulation corresponding to System (3) is :

$$L_\nu(\vec{x}, \vec{u}) = \int_0^{+\infty} p_{\mathcal{L}}(l) dl \left[ \begin{array}{l} \mathcal{H}(\vec{x}' \notin \Omega) L_\nu^{\partial\Omega}(\vec{y}, \vec{u}) \\ + \mathcal{H}(\vec{x}' \in \Omega) \left[ \begin{array}{l} P_{\text{abs}}(\vec{x}') L_\nu^{\text{eq}}(T(\vec{x}')) \\ + P_{\text{sca}}(\vec{x}') \int_{4\pi} p_\nu(\vec{u}', \vec{u}) d\vec{u}' L_\nu(\vec{x}', \vec{u}') \end{array} \right] \end{array} \right], \quad (4)$$

with  $p_{\mathcal{L}}(l) = k_{\text{ext},\nu}(\vec{x} - l\vec{u}) e^{-\int_0^l k_{\text{ext},\nu}(\vec{x} - l'\vec{u}) dl'}$  the probability density function for sampling a free path of length  $l$ , which provides the next collision position  $\vec{x}' = \vec{x} - l\vec{u}$ . Equation (4) can be translated into a backward Monte Carlo algorithm that estimates  $L_\nu(\vec{x}, \vec{u})$  as a sum of contributions from emission sources. Each collision position  $\vec{x}'$  is either outside the medium ( $\mathcal{H}(\vec{x}' \notin \Omega)$ ), in which case the retained weight is  $L_\nu^{\partial\Omega}(\vec{y}, \vec{u})$  (the boundary condition radiance in direction  $\vec{u}$  and at position  $\vec{y}$ ,  $\vec{y}$  being the position of the first intersection between the  $(\vec{x}, \vec{u})$  sightline and the boundary  $\partial\Omega$ ), or  $\vec{x}'$  is still in the medium ( $\mathcal{H}(\vec{x}' \in \Omega)$ ) (see Figure 1). In the latter case, two types of collision events can take place according to probabilities  $P_{\text{abs}}(\vec{x}) = k_{a,\nu}(\vec{x})/k_{\text{ext},\nu}(\vec{x})$  and  $P_{\text{sca}}(\vec{x}) = k_{s,\nu}(\vec{x})/k_{\text{ext},\nu}(\vec{x})$  for an absorption event or a scattering event, respectively. In the case of an absorption event, the Monte Carlo weight is the blackbody equilibrium radiance  $L_\nu^{\text{eq}}(T(\vec{x}'))$  at the  $\vec{x}'$  collision position. This is because absorption points in a reverse path correspond to emission points in its corresponding forward path, leveraging the reciprocity of light paths in accordance with the second law of thermodynamics. In the case of a scattering event, the optical trajectory continues in a new propagation direction  $\vec{u}'$  sampled according to the phase function  $p_\nu(\vec{u}', \vec{u})$ . Radiance  $L_\nu(\vec{x}', \vec{u}')$  for the new position and propagation direction

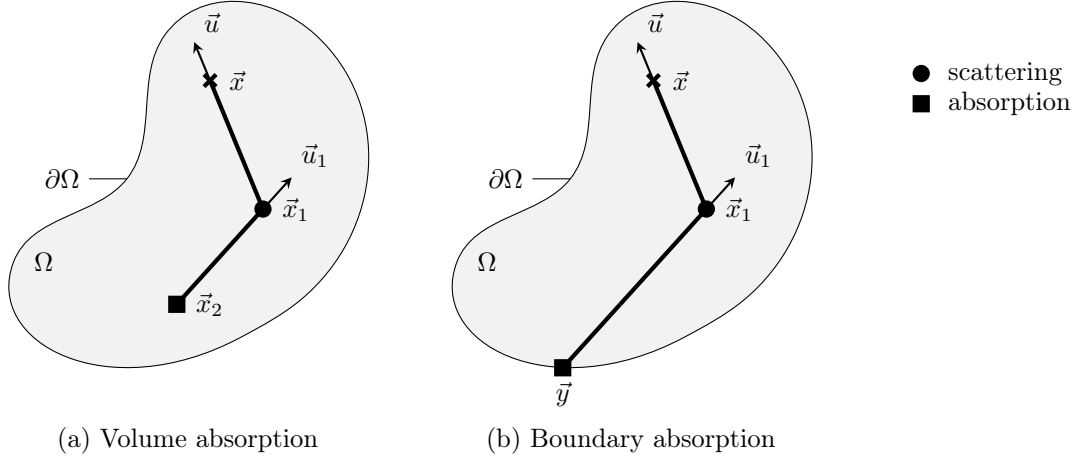


Figure 1: An example of radiance reverse path starting at  $\vec{x}$  in direction  $\vec{u}$  is shown. It is composed of several scattering events (circle) before finally reaching an absorption event (square) occurring either (a) in the volume  $\Omega$ , or (b) at the system boundary  $\partial\Omega$ . Absorption points in a reverse path correspond to emission points in its corresponding forward path, leveraging the reciprocity of light paths in accordance with the second law of thermodynamics.

has to be computed.  $L_\nu(\vec{x}', \vec{u}')$  has the very same integral formulation as  $L_\nu(\vec{x}, \vec{u})$ : the path-integral formulation is recursive.

The probabilistic model above presents two difficulties. The first one is encountered when sampling the extinction length  $l$ , as  $L_\nu(\vec{x}, \vec{u})$  depends non-linearly (through an exponential function) on the integral of the heterogeneous extinction coefficient field  $k_{ext,\nu}(\vec{x})$ . The second one is encountered when sampling the collision type; the absorption coefficient is a sum over millions of molecular transitions:  $k_{a,\nu}(\vec{x}) = \sum_{j=1}^{N_t} h_{a,\nu,j}(\vec{x})$  with  $h_{a,\nu,j}(\vec{x})$  the contribution of transition of index  $j$  to the total absorption coefficient of the medium; this is computationally expensive to estimate. Approximation methods for the calculation of the absorption coefficient field exist and are routinely used in atmospheric radiative transfer, but their model errors can be difficult to quantify. Interestingly, using the null-collision method makes both of these limitations vanish [12]. Not only does introducing fictive colliders homogenize the extinction coefficient field [15, 16] making the sampling of the extinction length  $l$  simpler, but it also enables a coupling between the line-by-line spectroscopic model and the radiative transfer model [6, 14], where the absorption coefficient is replaced with a transition sampling over the spectral domain. The resulting model now encompasses radiation and spectroscopy in a single path-integral formulation. In terms of model resolution, the model is simulated as a whole in a single Monte Carlo simulation [6]. This particular point becomes more obvious through the algorithmic illustration given in section 2.3, which is the probabilistic description of the following path-integral formulation, derived in Appendix A:

$$L_\nu(\vec{x}, \vec{u}) = \int_0^{+\infty} \hat{p}_{\mathcal{L}}(l) dl \left[ \begin{array}{l} \mathcal{H}(\vec{x}' \notin \Omega) L_\nu^{\partial\Omega}(\vec{y}, \vec{u}) \\ + \mathcal{H}(\vec{x}' \in \Omega) \left[ \begin{array}{l} \hat{P}_s \left\{ \begin{array}{l} P_s(\vec{x}') \int_{4\pi} p_\nu(\vec{u}', \vec{u}) d\vec{u}' L_\nu(\vec{x}', \vec{u}') \\ + (1 - P_s(\vec{x}')) L_\nu(\vec{x}', \vec{u}) \end{array} \right\} \\ + (1 - \hat{P}_s) \left( \sum_{j=1}^{N_t} P_J(j, \nu) \left\{ \begin{array}{l} P_{a,j}(\vec{x}') L_\nu^{eq}(T(\vec{x}')) \\ + (1 - P_{a,j}(\vec{x}')) L_\nu(\vec{x}', \vec{u}) \end{array} \right\} \right) \end{array} \right] \end{array} \right] \quad (5)$$

where the different terms  $\hat{P}_\square$  and  $P_\square$  are introduced to account for null collisions (see Appendix

A).

This reformulation results in a path-integral where the physics of radiative transfer is nonlinearly coupled to spectroscopy through the introduction of recursive null events. The requirement of pre-computing the absorption coefficient field is shifted to the ability to sample just one transition per one Monte Carlo realization.

Indeed, Equation 5 can be translated into a Monte Carlo algorithm, for which the procedure for one realization is presented in Algorithm 1. The optical path associated with each realization can propagate in the medium without knowing the real extinction coefficient field upfront, because it is needed only locally at each collision location. To sample a collision location, only a number of homogeneous upper bound free parameters are required to define various probabilities:  $\hat{k}_{a,\nu}$  is an upper-bound of the absorption coefficient field,  $\hat{k}_{s,\nu}$  is an upper-bound of the scattering coefficient field and  $\hat{k}_{ext,\nu} = \hat{k}_{a,\nu} + \hat{k}_{s,\nu}$  is an upper-bound of the extinction coefficient field. An upper-bound  $\hat{h}_{a,\nu,j}$  of the contribution  $h_{a,\nu,j}(\vec{x})$  of transition of index  $j$  to the local absorption coefficient must also be defined, so that  $\hat{k}_{a,\nu} = \sum_{j=1}^{N_t} \hat{h}_{a,\nu,j}$ , where  $N_t$  is the total number of transitions. As we will see in next section, we obtain a path-integral of a similar structure for sensitivities, for which we provide a complete description in the algorithmic section.

As far as computational cost is concerned, arbitrarily choosing these uniform upper-bound free parameters does not necessarily ensure an efficient sampling of transitions because absorption spectra are highly varying in frequencies. This can lead to a significant computational cost if chosen too large compared to the true absorption spectra: as  $\hat{k}_{ext,\nu}$  increases relative to  $k_{ext,\nu}(\vec{x})$ , sampled path-lengths  $l$  become shorter, and the likelihood of encountering null events increases. Consequently, this necessitates the sampling of a considerable number of consecutive spatial positions to sample a single path. This is where computer scientists' expertise in structuring and processing data comes into play. For an efficient sampling of large spectral data sets, the frequency domain is partitioned inside a hierarchical grid to build a field of upper bounds adapted to the absorption spectra variations. This data structuring makes the computational cost weakly sensitive to the size [5, 16] (number of transitions) and the complexity (shape of absorption spectra) of the spectroscopic database. Given the significant variability of absorption spectra with altitude, mostly due to pressure variations, the spectral hierarchical grids are tabulated as a function of pressure, and algorithmic adjustments are designed such that no alterations are made to the integral formulation represented by Equation 5.

The next section details the formal developments for obtaining a similar path-integral for sensitivities.

## 2.2 Estimating global radiative flux sensitivities

The previous section establishes the path-integral Monte Carlo approach for evaluating the global outgoing radiative flux at TOA using an integral reformulation for radiance. In this section, we show how to extend this framework to estimate flux sensitivities, paying specific attention to retaining the benefits associated with the use of the null-collision technique.

Sensitivity with respect to parameter  $\bar{\pi}$  is defined as  $\partial_{\bar{\pi}}\bar{\phi}$  the partial derivative of the flux at TOA. Let  $s_\nu$  be defined such that  $s_\nu(\vec{x}, \vec{u}, t, \bar{\pi}) = \partial_{\bar{\pi}}L_\nu(\vec{x}, \vec{u}, t, \bar{\pi})$ , then the TOA flux sensitivity is:

$$\partial_{\bar{\pi}}\bar{\phi} = \int_{\Delta t} p_T(t)dt \int_S p_S(\vec{x})dS(\vec{x}) \int_0^{+\infty} p_N(\nu)d\nu \int_{2\pi} p_U(\vec{u})d\vec{u} \left\{ \frac{\pi s_\nu(\vec{x}, \vec{u}, t, \bar{\pi})}{p_N(\nu)} \right\}, \quad (6)$$

which requires a path-integral formulation of  $s_\nu$ , similar to the path-integral formulation that was

required for  $L_\nu$  in the previous section. In addressing the question of sensitivity estimation using Monte Carlo methods, two different approaches may be considered. The first one consists in differentiating the path-integral formulation of  $L_\nu(\vec{x}, \vec{u})$  in Equation (5), and rewriting the resulting integral in order to preserve the same random samplings (and thus, the same algorithmic structure) between the quantity and its derivatives [10]. This is computationally efficient since only one set of paths has to be sampled to estimate all the quantities at once. However, when null-collision algorithms are implemented in combination with acceleration structures to guarantee that only a small fraction of fictive colliders is introduced at any location, [17] has demonstrated that the variance of the sensitivity estimates might be unbounded. This is because the weights that are retained for the sensitivity estimates are inversely proportional to the concentration of fictive colliders, which tends to zero as the acceleration structure is better optimized. [17] proposed a solution to bypass this difficulty, but this requires an additional sampling at each collision event. The second approach, which we choose to explore in the present work, consists in differentiating the radiative transport model of  $L_\nu(\vec{x}, \vec{u})$  in System (3) to establish a transport model for the sensitivity. This method was originally developed for geometric sensitivities (derivatives with respect to parameters the geometry depends upon [18, 19]) and it will be used hereafter for parametric (non-geometric) sensitivities. This framework enables the physical analysis of sensitivity propagation in the participating medium.

According to the second approach, differentiating System (3) with respect to  $\vec{\pi}$  yields a transport model for the sensitivity that can be expressed using a new transport equation, namely a Sensitivity Transport Equation (STE):

$$\left\{ \begin{array}{l} \forall \vec{x} \in \Omega, \forall \vec{u} \in \mathbf{S}^2 : \\ \vec{u} \cdot \vec{\nabla}_X s_\nu(\vec{x}, \vec{u}, \vec{\pi}) = -k_{ext,\nu}(\vec{x}, \vec{\pi}) s_\nu(\vec{x}, \vec{u}, \vec{\pi}) + k_{a,\nu}(\vec{x}, \vec{\pi}) \left[ \frac{\partial_{\vec{\pi}} k_{a,\nu}(\vec{x}, \vec{\pi})}{k_{a,\nu}(\vec{x}, \vec{\pi})} (L_\nu^{eq}(T(\vec{x})) - L_\nu(\vec{x}, \vec{u}, \vec{\pi})) \right] \\ \quad + k_{s,\nu}(\vec{x}, \vec{\pi}) \int_{4\pi} p_\nu(\vec{u}', \vec{u}) d\vec{u}' (s_\nu(\vec{x}, \vec{u}', \vec{\pi}) + \left[ \frac{\partial_{\vec{\pi}} k_{s,\nu}(\vec{x}, \vec{\pi})}{k_{s,\nu}(\vec{x}, \vec{\pi})} (L_\nu(\vec{x}, \vec{u}', \vec{\pi}) - L_\nu(\vec{x}, \vec{u}, \vec{\pi})) \right]) \\ \forall \vec{y} \in \partial\Omega, \forall \vec{u}_+ \in \mathbf{S}_+^2 : \\ s_\nu(\vec{y}, \vec{u}_+) = 0 \end{array} \right. \quad (7)$$

Comparing STE (Equation 7) with RTE (Equation 3), we see that the structure for transport of sensitivity is very similar to that of radiance, which translates into the same sampling procedure between the two quantities. The difference only regards the sources via absorption and scattering.

At this point, the STE can be solved using any model for the absorption and scattering coefficients fields  $k_{a,\nu}(\vec{x}, \vec{\pi})$  and  $k_{s,\nu}(\vec{x}, \vec{\pi})$ . However, it is possible to establish a sensitivity model that couples line-by-line spectroscopy and radiative transfer, following the same formal developments (in Appendix A) used for the construction of the multiphysics model of radiance. Doing so, we obtain a path-integral formulation for sensitivity similar to the path-integral formulation for radiance in Equation 5:



$$\begin{aligned}
s_\nu(\vec{x}, \vec{u}, \vec{\pi}) &= \int_0^{+\infty} \hat{p}_{\mathcal{L}}(l) dl \\
&\left[ \begin{array}{l} \mathcal{H}(\vec{x}' \notin \Omega) \cdot 0 \\ + \mathcal{H}(\vec{x}' \in \Omega) \\ \left[ \begin{array}{l} \hat{P}_s(\vec{x}') \left\{ P_s(\vec{x}') \int_{4\pi} p_\nu(\vec{u}', \vec{u}) d\vec{u}' \left[ s_\nu(\vec{x}', \vec{u}', \vec{\pi}) + \left[ \frac{\partial_{\vec{\pi}} k_{d,\nu}(\vec{x}, \vec{\pi})}{k_{d,\nu}(\vec{x}, \vec{\pi})} (L_\nu(\vec{x}', \vec{u}', \vec{\pi}) - L_\nu(\vec{x}', \vec{u}, \vec{\pi})) \right] \right\} \right. \\ \left. + (1 - P_s(\vec{x}')) [s_\nu(\vec{x}', \vec{u}, \vec{\pi})] \right. \\ \left. + (1 - \hat{P}_s(\vec{x}')) \left( \sum_{j=1}^{N_t} P_J(j, \nu) \left\{ P_{a,j}(\vec{x}') \left[ \frac{\partial_{\vec{\pi}} h_{a,\nu,j}(\vec{x}, \vec{\pi})}{h_{a,\nu,j}(\vec{x}, \vec{\pi})} (L_\nu^{eq}(T(\vec{x}')) - L_\nu(\vec{x}', \vec{u}, \vec{\pi})) \right] \right\} \right) \right. \\ \left. + (1 - P_{a,j}(\vec{x}')) [s_\nu(\vec{x}', \vec{u}, \vec{\pi})] \right. \end{array} \right] \end{array} \right] \quad (8)
\end{aligned}$$

The resulting path-integral formulation can correspond to multiple Monte Carlo algorithmic interpretations. We will now elaborate on the specificities of our simulation choices.

### 2.3 From path-integral formulation to Monte Carlo algorithm

We can read in our sensitivity path-integral formulation (Equation 8) a coupling to two other path-integrals corresponding to two distinct physics. The first coupling is to the line-by-line spectroscopic model through  $P_{a,j}$ , governing real or null transitions. The second coupling is to the radiance model  $L_\nu$ , which appears in the weights of sensitivity Monte Carlo realizations. We refer to these through *coupling* because the sensitivity path-integral is designed in a way that a single Monte Carlo iteration walks across different physics by sampling their associated random variables — here, radiance and absorption coefficient — without requiring their explicit resolution. Instead, only one realization of each corresponding random variable is sampled.

This becomes manifest in the statistical procedure for sampling a single Monte Carlo weight presented in Algorithm 2, which is a strict translation of the sensitivity path-integral formulation presented in Equation 8. The complete Monte Carlo for sensitivity estimation entails  $N$  averaged realizations, each sampled as follows:

- Initialization: start an optical path at position  $\vec{x}$ , in direction  $-\vec{u}$ .
- Sampling path length: sample path length  $l$  according to  $\hat{p}_{\mathcal{L}}(l) = \hat{k}_{ext,\nu} \exp(-\hat{k}_{ext,\nu} l)$  over  $[0, +\infty)$ .
- Update position :  $\vec{x}' = \vec{x} - l\vec{u}$ .
- Boundary check: check whether  $\vec{x}'$  is outside or inside  $\Omega$ .
  - If outside, the weight is the boundary condition (here it is null because the boundary conditions in the model of  $L$  was set independent of the parameter), and the realization stops.
  - If inside, proceed to collision branch determination at  $\vec{x}'$ .
- Collision branch determination: determine the collision type by sampling between the *scattering branch* and the *absorption branch* with probabilities  $\hat{P}_s(\vec{x}')$  and  $\hat{P}_a(\vec{x}') = 1 - \hat{P}_s(\vec{x}')$ , respectively.
- If the "scattering branch" is selected: determine whether it is a real or a null scattering event with probabilities  $P_s(\vec{x}')$  and  $1 - P_s(\vec{x}')$ , respectively.
  - If real scattering event: the new propagation direction  $\vec{u}'$  has to be sampled over  $4\pi$  sr according to the  $p(\vec{u}', \vec{u})$  probability density. Then we evaluate  $s_\nu(\vec{x}', \vec{u}', \vec{\pi})$  by recursing on Algorithm 2; we also evaluate  $L_\nu(\vec{x}', \vec{u}', \vec{\pi})$  and  $L_\nu(\vec{x}', \vec{u}, \vec{\pi})$  using Algorithm 1 via double

randomization, meaning we estimate one Monte Carlo realization of Algorithm 1 at position  $\vec{x}'$  and direction  $\vec{u}'$  and at  $\vec{x}'$  and direction  $\vec{u}$ , respectively. The Monte Carlo weight we retain is then  $s_\nu(\vec{x}', \vec{u}', \vec{\pi}) + \left[ \frac{\partial_{\vec{\pi}} k_{d,\nu}(\vec{x}, \vec{\pi})}{k_{d,\nu}(\vec{x}, \vec{\pi})} (L_\nu(\vec{x}', \vec{u}', \vec{\pi}) - L_\nu(\vec{x}', \vec{u}, \vec{\pi})) \right]$ , and additional data has to be known at this point: the value of  $\partial_{\vec{\pi}} k_{d,\nu}(\vec{x}, \vec{\pi})$ .

- If null scattering event: recurse on Algorithm 2 at the new position  $\vec{x}'$  but in the same direction  $\vec{u}$ .
- If the "absorption branch" is selected: sample a transition according to the  $P_J(j, \nu) = \frac{\hat{h}_{a,j,\nu}}{\hat{k}_{a,\nu}}$ ,  $j \in [1, N_t]$  probability set. Then determine whether it is a real or a null transition event with probabilities  $P_{a,j}(\vec{x}') = \frac{h_{a,j}(\vec{x})}{\hat{h}_{a,j,\nu}}$  and  $1 - P_{a,j}(\vec{x}') = \frac{\hat{h}_{a,j} - h_{a,j}(\vec{x})}{\hat{h}_{a,j,\nu}}$ , respectively.
  - If real transition event: the weight  $\frac{\partial_{\vec{\pi}} h_{a,\nu,j}(\vec{x}, \vec{\pi})}{h_{a,\nu,j}(\vec{x}, \vec{\pi})} (L_\nu^{eq}(T(\vec{x}')) - L_\nu(\vec{x}', \vec{u}, \vec{\pi}))$  is retained and the realization stops. Two additional quantities need to be evaluated: the value of  $\partial_{\vec{\pi}} h_{a,\nu,j}(\vec{x}, \vec{\pi})$  and  $L_\nu(\vec{x}', \vec{u}, \vec{\pi})$ . The latter is evaluated by a single realization of the corresponding radiance random variable, relying on double randomization.
  - If null transition event: recurse on Algorithm 2 at the new position  $\vec{x}'$  but in the same direction  $\vec{u}$ .

---

### Algorithm 1 Radiance realization $L_\nu(\vec{x}, \vec{u}, \vec{\pi})$

---

**Input:** a position  $\vec{x}$ , a direction  $\vec{u}$ , a parameter  $\vec{\pi}$

**Output:** a Monte Carlo radiance weight  $\omega$

**function** RADIANCEREALIZATION( $\vec{x}, \vec{u}, \vec{\pi}$ )

  Sample a length to the next collision position  $l$  according to  $\hat{p}_L(l)$

  Compute the next collision position  $\vec{x}' \leftarrow \vec{x} - l\vec{u}$

**if**  $\vec{x}' \notin \Omega$  **then**

    Compute position  $\vec{y}$  of intersection between  $(\vec{x}, -\vec{u})$  ray and boundary  $\partial\Omega$

$\omega \leftarrow L_\nu^{\partial\Omega}(\vec{y}, \vec{u})$

**else**

    Sample a uniform random variable  $r \in [0, 1]$

**if**  $r < \hat{P}_s(\vec{x}')$  **then** /\* scattering \*/

      Sample a uniform random variable  $r \in [0, 1]$

**if**  $r < P_s(\vec{x}')$  **then** /\* real-scattering event \*/

        Sample scattering direction  $\vec{u}'$  according to phase function  $p(\vec{u}', \vec{u})$

$\omega \leftarrow \text{RADIANCEREALIZATION}(\vec{x}', \vec{u}', \vec{\pi})$

▷ **Recurse** Algo. 1

**else** /\* null-scattering event \*/

$\omega \leftarrow \text{RADIANCEREALIZATION}(\vec{x}', \vec{u}, \vec{\pi})$

▷ **Recurse** Algo. 1

**end if**

**else** /\* absorption \*/

      Sample a transition  $j$  according to  $P_J(j, \nu)$

      Sample a uniform random variable  $r \in [0, 1]$

**if**  $r < P_{a,j}(\vec{x}')$  **then** /\* real-transition event \*/

$\omega \leftarrow L_\nu^{eq}(T(\vec{x}'))$

**else** /\* null-transition event \*/

$\omega \leftarrow \text{RADIANCEREALIZATION}(\vec{x}', \vec{u}, \vec{\pi})$

▷ **Recurse** Algo. 1

**end if**

**end if**

**end if**

**return**  $\omega$

**end function**

---

---

**Algorithm 2** Sensitivity realization  $s_\nu(\vec{x}, \vec{u}, \vec{\pi})$ 


---

**Input:** a position  $\vec{x}$ , a direction  $\vec{u}$ , a parameter  $\vec{\pi}$

**Output:** a Monte Carlo sensitivity weight  $\omega$

**function** SENSITIVITYREALIZATION( $\vec{x}, \vec{u}, \vec{\pi}$ )

  Sample a length to the next collision position  $l$  according to  $\hat{p}_L(l)$

  Compute the next collision position  $\vec{x}' \leftarrow \vec{x} - l\vec{u}$

**if**  $\vec{x}' \notin \Omega$  **then**

$\omega \leftarrow 0$

**else**

    Sample a uniform random variable  $r \in [0, 1]$

**if**  $r < \hat{P}_s(\vec{x}')$  **then** /\* scattering \*/

      Sample a uniform random variable  $r \in [0, 1]$

**if**  $r < P_s(\vec{x}')$  **then** /\* real-scattering event \*/

        Sample scattering direction  $\vec{u}'$  according to phase function  $p(\vec{u}', \vec{u})$

$L_\nu(\vec{x}', \vec{u}', \vec{\pi}) \leftarrow \text{RADIANCEREALIZATION}(\vec{x}', \vec{u}', \vec{\pi})$

▷ Algo. 1

$L_\nu(\vec{x}', \vec{u}, \vec{\pi}) \leftarrow \text{RADIANCEREALIZATION}(\vec{x}', \vec{u}, \vec{\pi})$

▷ Algo. 1

$s_\nu(\vec{x}', \vec{u}', \vec{\pi}) \leftarrow \text{SENSITIVITYREALIZATION}(\vec{x}', \vec{u}', \vec{\pi})$

▷ **Recurse** Algo. 2

$\omega \leftarrow s_\nu(\vec{x}', \vec{u}', \vec{\pi}) + \frac{\partial_{\vec{\pi}} k_{d,\nu}(\vec{x}, \vec{\pi})}{k_{d,\nu}(\vec{x}, \vec{\pi})} (L_\nu(\vec{x}', \vec{u}', \vec{\pi}) - L_\nu(\vec{x}', \vec{u}, \vec{\pi}))$

**else** /\* null-scattering event \*/

$\omega \leftarrow \text{SENSITIVITYREALIZATION}(\vec{x}', \vec{u}, \vec{\pi})$

▷ **Recurse** Algo. 2

**end if**

**else** /\* absorption \*/

      Sample a transition  $j$  according to  $P_J(j, \nu)$

      Sample a uniform random variable  $r \in [0, 1]$

**if**  $r < P_{a,j}(\vec{x}')$  **then** /\* real-transition event \*/

        Compute equilibrium blackbody radiance  $L_\nu^{eq}(T(\vec{x}'))$

$L_\nu(\vec{x}', \vec{u}, \vec{\pi}) \leftarrow \text{RADIANCEREALIZATION}(\vec{x}', \vec{u}, \vec{\pi})$

▷ Algo. 1

$\omega \leftarrow \frac{\partial_{\vec{\pi}} h_{a,\nu,j}(\vec{x}, \vec{\pi})}{h_{a,\nu,j}(\vec{x}, \vec{\pi})} (L_\nu^{eq}(T(\vec{x}')) - L_\nu(\vec{x}', \vec{u}, \vec{\pi}))$

**else** /\* null-transition event \*/

$\omega \leftarrow \text{SENSITIVITYREALIZATION}(\vec{x}', \vec{u}, \vec{\pi})$

▷ **Recurse** Algo. 2

**end if**

**end if**

**end if**

**return**  $\omega$

**end function**

---

This algorithmic efficiency is facilitated by leveraging a mathematical statistical property encapsulated in Box 2.3, initially introduced in the work [30]. In our model, this property is particularly relevant, as sensitivity, akin to radiance, shares a structural similarity with  $g$  in Box 2.3. This arises from specific formal development choices made during the construction of Equation 8 for sensitivity (and Equation 5 for radiance). To draw a parallel, sampling a single realization of  $X$  to determine the Bernoulli parameter  $P = \frac{X}{x}$  in the Box — instead of computing its expectation —, is the theoretical justification in our model for sampling a single transition to determine the absorption probability — instead of pre-computing the absorption coefficient — [16]. Subsequently, a Bernoulli trial follows to determine whether it corresponds to a real or null absorption, thus retaining the corresponding sensitivity weight (or radiance weight).

### Box : A mathematical property for our statistical framework

This box demonstrates that if  $g$  is the expectation of a Bernoulli random variable (with possible outcomes  $\mathbb{E}(Y)$  and  $\mathbb{E}(Z)$ ) where the probability is itself the expectation of a random variable  $\frac{X}{\hat{x}}$  whose domain is the interval  $[0, 1]$ , then the expectation of  $W$  is an unbiased estimator for  $g$ , where a single realization of  $\frac{X}{\hat{x}}$  is sampled for each realization of  $W$ .

**Property:** Let  $g$  be a function of the expectancy of random variables  $X$ ,  $Y$ , and  $Z$ , defined by the following structure:

$$g = \frac{\mathbb{E}(X)}{\hat{x}} \cdot \mathbb{E}(Y) + \left[ 1 - \frac{\mathbb{E}(X)}{\hat{x}} \right] \cdot \mathbb{E}(Z)$$

where  $\hat{x}$  is an upper bound for *all* realizations  $x$  of  $X$ .

Then  $g$  is the expectation of random variable  $W$ :

$$g = \mathbb{E}(W)$$

such that:

$$W = B\left(\frac{X}{\hat{x}}\right) \cdot Y + \left[ 1 - B\left(\frac{X}{\hat{x}}\right) \right] \cdot Z$$

where  $B\left(\frac{X}{\hat{x}}\right)$  is the Bernoulli variable of parameter the random variable  $P = \frac{X}{\hat{x}}$ .

**Demonstration:** By definition of  $g$ , we have:

$$g = \frac{\int_{D_X} x p_X(x) dx}{\hat{x}} \cdot \int_{D_Y} y p_Y(y) dy + \left[ 1 - \frac{\int_{D_X} x p_X(x) dx}{\hat{x}} \right] \cdot \int_{D_Z} z p_Z(z) dz$$

with  $p_X$ ,  $p_Y$  and  $p_Z$  the probability density functions associated to random variables  $X$ ,  $Y$  and  $Z$ , respectively.

It can be reformulated as:

$$g = \int_{D_X} p_X(x) dx \left( \frac{x}{\hat{x}} \cdot \int_{D_Y} y p_Y(y) dy + \left[ 1 - \frac{x}{\hat{x}} \right] \cdot \int_{D_Z} z p_Z(z) dz \right)$$

Figure 2 illustrates a sensitivity path in pink, consisting of a sequence of consecutive collision events. The physics coupling is visually conveyed through path branches, with the rainbow representing the spectroscopy and yellow representing the radiance model. The distinct nature of these two physics branches is particularly noteworthy. The spectroscopic rainbow branch contributes to constructing the sensitivity path, determining whether it continues beyond a collision site in the absorption branch. In contrast, each yellow radiance branch samples information that will contribute to the sensitivity Monte Carlo weight but not to the construction of the sensitivity path. This difference in the two coupling statuses is grounded in the differential form of the STE. On the one hand, the sensitivity transport model exhibits a non-linear dependency on the absorption coefficient through Beer's exponential, which is bypassed using null collisions. On the other hand, the radiance appears as a volumetric source term in the STE, hence the linearity of the radiance-sensitivity coupling.

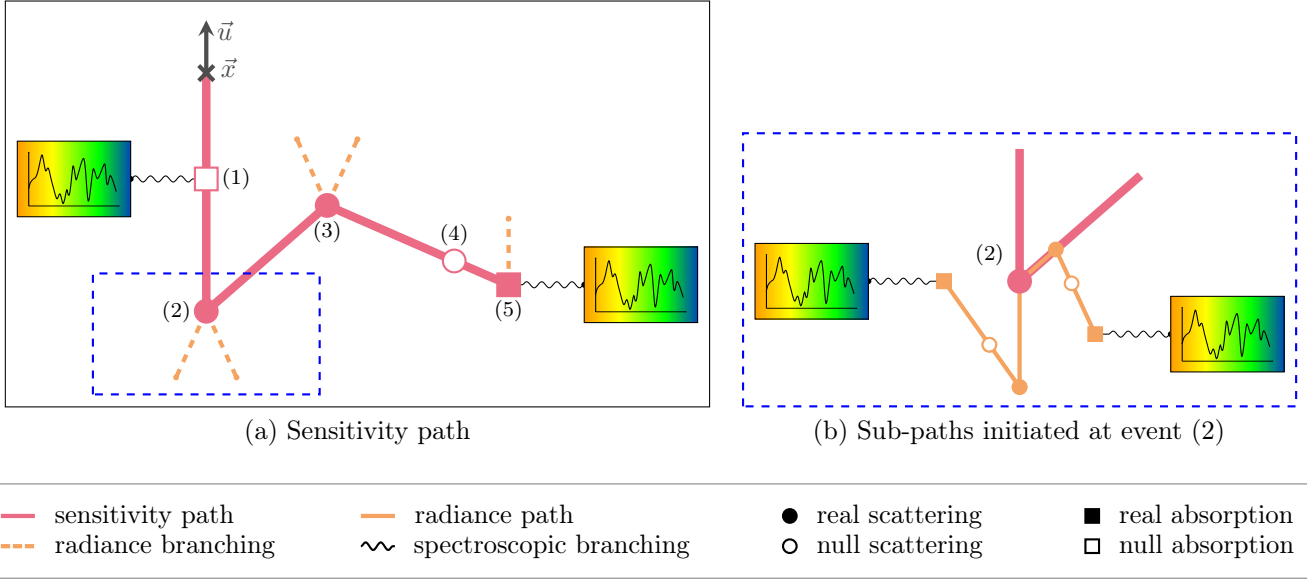


Figure 2: On the left side, we depict an instance of the sensitivity reverse path in pink, starting at point  $\vec{x}$  in direction  $\vec{u}$ . The nodes along the path represent real (filled) or null (empty) events of two distinct types: scattering (circle) or absorption (square). Along the sensitivity path, branching sub-paths emerge at these nodes based on their type, invoking either spectroscopic sub-paths in rainbow, radiance sub-paths in yellow, or both. This specific sensitivity path consists of five events. (1) is an absorption event that was randomly determined as being null after sampling a transition where a rainbow spectroscopic sub-path was launched to determine the event type; (2) is a real scattering event; in this case, two yellow radiance sub-paths were launched as a contribution to the path weight; (3) is a similar real scattering event; (4) is a null scattering event without sub-path branchings and (5) is an absorption event that was randomly determined as being real after sampling a transition where a rainbow spectroscopic sub-path was launched to determine the event type, and in this case, a yellow radiance sub-path was launched as a contribution to the path weight. The right panel displays a zoom on scattering event (2): radiance paths are similar to those of sensitivity but only contain rainbow spectroscopic branchings for path construction.

## 3 Results and discussions

### 3.1 Results

In the following, we will use as the inputs of our spectro-radiative model atmospheric state outputs from a simulation performed with the IPSL General Circulation Model 3.1. The IPSL climate model simulation was performed on a 144 x 143 longitude-latitude grid using 79 vertical levels. We use 3-hourly outputs of a 10-year simulation, which amounts to a total of 144x143x10x365x8  $\approx$  600 million columns [21]. The computations are performed in clear sky conditions considering four greenhouse gases (H<sub>2</sub>O, CO<sub>2</sub>, O<sub>3</sub>, and CH<sub>4</sub>), and using a line-by-line spectroscopic model with parameters sourced from the HITRAN database [19]. The Lorentz function describes the profile lineshapes, truncated at 25 cm<sup>-1</sup> for H<sub>2</sub>O, O<sub>3</sub>, CH<sub>4</sub>, and 50 cm<sup>-1</sup> for CO<sub>2</sub>. Analytical Lorentz profiles are used here, but the methodology extends to Voigt profiles with no further conceptual challenges. Also, the water vapor continuum is not accounted for in the present simulations, and its inclusion would similarly present no further conceptual difficulties.

The theoretical developments are applicable to any parameter of interest in the spectro-radiative model. Here, we focus on the radiative forcings resulting from a fractional change in greenhouse gas concentration. Therefore, we define a sensitivity parameter  $\tilde{\pi}$  that acts on the concentration fields and consequently on radiative fluxes through molecular transitions  $h_{a,\nu,j}(\vec{x}, \tilde{\pi})$  as a multiplier factor of the reference molar fraction of gas, i.e.,  $x_{\text{gas}} = \tilde{\pi} \times x_{\text{gas, ref}}$ . The initial concentration of carbon dioxide is set to the pre-industrial era value  $x_{\text{CO}_2, \text{ref}} = 280$  ppm. Each spectral line of index  $j$  is modelled as the product of molecular density  $n$ , line intensity  $S_j$ , and line profile  $f_{\nu,j}$ . The dependence on parameter  $\tilde{\pi}$  intervenes in molecular density  $n(\vec{x}, \tilde{\pi})$  and line profile  $f_{\nu,j}(\vec{x}, t, \tilde{\pi})$ . The derivative of a spectral line  $h_{a,\nu,j}(\vec{x}, \tilde{\pi})$  with respect to  $\tilde{\pi}$  is then given by:

$$\partial_{\tilde{\pi}} h_{a,\nu,j}(\vec{x}, \tilde{\pi}) = S_j(\vec{x}, t) \partial_{\tilde{\pi}} [n(\vec{x}, \tilde{\pi}) f_{\nu,j}(\vec{x}, t, \tilde{\pi})] \quad (9)$$

Using Algorithm 1, we obtain the integrated TOA mean flux  $\bar{\phi}$  depicted in Fig. 3a, Fig. 3c, and Fig. 3e. Using Algorithm 2, we obtain the integrated TOA mean flux sensitivity  $\partial_{\tilde{\pi}} \bar{\phi}$  shown in Fig. 3b, Fig. 3d, and Fig. 3f, with respect to parameter values  $\tilde{\pi}$  affecting CO<sub>2</sub>, H<sub>2</sub>O, and CH<sub>4</sub>. The figures illustrate these quantities as a function of parameter values  $\tilde{\pi}$ . Each point corresponds to an independent estimation, conducted globally over a month and spanning the thermal infrared range [100; 2500] cm<sup>-1</sup> with  $N = 640\,000$  Monte Carlo realizations each.

Fig. 4 represents the dependence of computational time required for achieving a 1% relative error on sensitivity estimates (on a personal computer with 12 CPUs), as a function of the widening in the spectral, spatial and temporal integration domains.

### 3.2 Discussions

In discussing the results, we focus on three key aspects: (i) in Section 3.2.1, we address the advantages of estimating sensitivity through path-integral Monte Carlo simulations compared to finite differences methods; (ii) in Section 3.2.2, we analyze the computation times as the integration domains are widened; and (iii) in Section 3.2.3, we validate our methods by comparing our results to a well-established functional dependency of the global TOA radiative flux upon fraction change in carbon dioxide concentrations.

### 3.2.1 On sensitivity estimation

For a given gas and across all values of  $\bar{\pi}$ , the perturbation of  $\bar{\pi}$  we considered in the results corresponds to injecting the same infinitesimal amount  $dx_{\text{gas}} = x_{\text{gas, ref}} \times d\bar{\pi}$  of gas into the atmosphere. The resulting sensitivity is  $\partial_{\bar{\pi}}\bar{\phi}$ , the variation in the global outgoing flux at TOA. As anticipated, the negative sensitivities reflect the expected decrease in outgoing flux with an increase in greenhouse gas concentration, in line with the greenhouse effect. Comparing forcings due to different gases, a higher forcing from a gas corresponds to a greater expected impact when increasing its concentration, consistent with the obtained sensitivities; water vapor exhibits larger sensitivities than carbon dioxide and methane, given its greater abundance (see Fig. 3d and Fig. 3f).

For water vapor and carbon dioxide, the finite differences resulting from two distinct Monte Carlo estimations of the flux provide reasonably accurate approximations of the estimated path-integral sensitivities. However, for methane, where variations in mean flux are small (see Fig. 3e), finite differences exhibit large fluctuations, contrasting with the more stable path-integral sensitivity estimates (see Fig. 3f). Moreover, Monte Carlo estimation provides unbiased sensitivities along with their statistical uncertainty, whereas the uncertainty of finite differences comes from the uncertainties of flux estimation mixed with the uncertainty due to the discretization choice, the latter being impossible to quantify in practice. Moreover, if we keep the same number of realizations, the finer the discretization parameter  $h$ , the more relevant the finite differences approximation becomes, but the larger the associated Monte Carlo variance, which increase proportionally to  $1/h^2$ :

$$\begin{aligned}\partial_{\bar{\pi}}\bar{\phi}(\bar{\pi}) &\approx \frac{\bar{\phi}(\bar{\pi} + h) - \bar{\phi}(\bar{\pi} - h)}{2h} \\ \sigma^2 [\partial_{\bar{\pi}}\bar{\phi}(\bar{\pi})] &\approx \frac{1}{4h^2} \{ \sigma^2[\bar{\phi}(\bar{\pi} + h)] + \sigma^2[\bar{\phi}(\bar{\pi} - h)] \}\end{aligned}\tag{10}$$

The advantage of the approach becomes clear: instead of substantially increasing the number of Monte Carlo realizations on flux estimates in order to obtain reliable estimations through finite differences, we propose to use unbiased path-integral formulations for direct sensitivity estimations.

### 3.2.2 On the computation time and Monte Carlo standard deviation

Figure 4 illustrates how  $t_{1\%}$ , the computational time required to achieve a 1% error on  $\partial_{\bar{\pi}}\bar{\phi}$  estimates for carbon dioxide, depends on the widening of the respective integration domains, on a personal computer with 12 CPUs. In the first plot, we consider a single atmospheric column and a specific date, for which the quantity  $t_{1\%}$  is represented as a function of spectral integration over a band of increasing width, ranging from  $10 \text{ cm}^{-1}$  (marked by the first red dot) to  $2400 \text{ cm}^{-1}$  (the entire infrared range shown in the last red dot). Moving to the middle and the last plots,  $\partial_{\bar{\pi}}\bar{\phi}$  is additionally integrated over spatial and time domains of increasing size, from 1 to 20 592 atmospheric columns and over a time period ranging from one day up to ten years, respectively.

First of all, on spectral integration, we observe from the first plot that computation time slightly increases with domain widening. Looking at the sensitivity path-integral in Equation 8, during the Monte Carlo sampling of carbon dioxide sensitivity, the retained weight values depend on the derivative of the spectral line for a given parameter  $\bar{\pi}$ , and thus on which concentration field it acts upon. The initial red dot on the graph corresponds to frequency integration within the  $15 \mu\text{m}$   $\text{CO}_2$  band. Subsequent red points, up to an integration width of  $100 \text{ cm}^{-1}$ , remain within same band. Consequently, computational time remains insensitive in this band. This comes as no surprise as  $\text{CO}_2$  contribution relative to other molecules is dominant in this band. However, as the integration domain

is enlarged, within spectral intervals devoid of CO<sub>2</sub> contribution, the sensitivity weight consistently tends to zero, due to contributions from other molecular species, such as H<sub>2</sub>O, O<sub>3</sub>, and CH<sub>4</sub>, that become dominant. Consequently, higher proportions of sensitivity weights yield null values as absorption becomes frequently attributed to these alternative molecules. This introduces a source of greater variance, necessitating additional Monte Carlo realizations to mitigate it, resulting in the observed increase in  $t_1\%$ . While Monte Carlo variance reduction techniques, such as importance sampling — in our case, to minimize the sampling of absorptions by H<sub>2</sub>O, O<sub>3</sub>, and CH<sub>4</sub>— offer a prospective avenue for strategically sampling sensitivity weights, it falls beyond the scope of the present work.

Concerning the second and third plots, we note that expanding both the spatial and temporal integration domains has a negligible impact on computational time, maintaining consistent performance within a range of a few tens of seconds. Now, upon closer examination, the transition from the second to the third plot, corresponding to the introduction of the additional integration domain over time, leads to a 25% reduction in computational cost (from  $\sim 40$  seconds to  $\sim 30$  seconds), which can be surprising. As a matter of fact, among the 2920 time points that are now considered, there might be more or less favourable cases in terms of variance, and hence convergence. If the expansion of a certain integration dimension is anticipated to decrease the *proportion* of cases with the highest variance, then the same level of statistical precision would require reduced computational costs. Therefore, an additional integration domain in Monte Carlo simulations may sometimes reduce computational costs, e.g. [29], as it seems to be the case here. This point remains under scrutiny.

We observe that in a general sense, for the same level of data resolution, estimating sensitivity for a given date and position on the entire frequency domain (last red point) is nearly as costly as estimating the result when integrating over the entire thermal infrared band, over the entire Earth, and over ten years (last green point).

### 3.2.3 From carbon dioxide sensitivity to its radiative forcing estimation

The central focus of this paper has revolved around developing spectro-radiative path-integrals for sensitivities, designed for unbiased Monte Carlo simulations. The approach avoids approximation schemes at both levels of physics modeling and simulation, thereby providing, for the first time, a method for reference estimations for sensitivities of radiative integrated fluxes to spectroscopic parameters. As a final prospect, we use the approach in the context of radiative forcings, on our simplified configuration.

It is well-known in climate science that the radiative forcing from carbon dioxide is approximately logarithmic in its concentration [24], a property further explained in recent studies [25]. Indeed, the sensitivity to a logarithmic change in its fraction concentration field can be approximated by a constant  $a$ :

$$\frac{d\bar{\phi}}{d \ln \left( \frac{x_{\text{gas}}}{x_{\text{gas,ref}}} \right)} = a \quad (11)$$

This translates in our model as a functional form independent of the initial concentration field  $x_{\text{gas,ref}}$ , as it can be reformulated solely as a function of the parameter  $\bar{\pi}$ , representing the fractional change:

$$\frac{d\bar{\phi}}{d \ln \left( \frac{x_{\text{gas}}}{x_{\text{gas,ref}}} \right)} = \frac{d\bar{\phi}}{d \ln (\bar{\pi})} = \frac{d\bar{\phi}}{d\bar{\pi}} \cdot \bar{\pi} \quad (12)$$



This functional dependence property of  $\text{CO}_2$  can now be illustrated using our Monte Carlo simulations by plotting the estimated sensitivity  $\partial_{\tilde{\pi}}\bar{\phi}$ , multiplied by  $\tilde{\pi}$ , against  $\tilde{\pi}$ . As illustrated in Fig. 5, this results indeed in a constant value. Our path-integral sensitivity approach thus provides an independent simulation of this logarithmic dependence.

As a matter of fact, we can also note that a single value of our sensitivity estimations — let’s choose  $a = -3.86 \pm 0.06$  found for  $\tilde{\pi} = 1$ , taken as a reference case — enables the estimation of carbon dioxide radiative forcing for any fractional change in its concentration, given its functional dependency property. For instance, the radiative forcing for a doubling of the carbon dioxide concentration field yields  $\Delta\bar{\phi} = a \ln(2) = -2.68 \pm 0.06 \text{ W/m}^2$ , consistent with recent literature estimates [22].

## 4 Conclusions

The intention of the present work was to develop a Monte Carlo approach that provides unbiased and efficient spectro-radiative sensitivity estimates. Notably, the approach is employed in the context of estimating atmospheric radiative forcings within a clear-sky simplified climate framework.

By applying Monte Carlo within this framework, we illustrate a well-known property in climate science—the logarithmic tendency of radiative forcing from carbon dioxide in relation to its concentration.

The methodology is constructed to remain unbiased at both levels of physics modeling and simulation. On the theoretical level, sensitivity is regarded as a transported quantity with its own propagation physics, for which a path-integral solution is constructed. In this regard, we build upon recent advances in coupling the radiative transfer model to the spectroscopic model in a non-linear manner through the absorption coefficient, which disappears from the resulting model. After the formal developments are elaborated, the corresponding probabilistic description is provided in algorithmic form.

The simulation results presented in the preceding section illustrate the practicality of the approach within high-dimensional configurations, such as a climate one. In this latter, the estimated quantity is integrated across the entire thermal infrared band, over the whole globe, and along a climate period of ten years. Thanks to advanced computer graphics techniques, achieving a precision of 1 percent on sensitivity estimates required only a few tens of seconds of computation time on a personal computer with 12 CPUs. Scalability is demonstrated, and while minor convergence variabilities arise depending on the widening of integration domains to maintain the same confidence interval, standard optimization avenues in Monte Carlo practice exist and can be considered based on specific needs. However, these optimizations were deliberately excluded from this article.

## 5 Acknowledgements

We acknowledge support from the Agence Nationale de la Recherche (ANR, grant MCG-RAD ANR-18-CE46-0012, <https://mcg-rad.ipsl.fr/>).

# A Spectro-radiative path-integral construction as a solution to the Radiative Transfer Equation

Starting from the monochromatic radiative transfer equation given in Equation 3, but written over a single sightline  $(\vec{x}, \vec{u})$  parameterized by distance  $l$ :

$$\frac{\partial L(\vec{x}, \vec{u})}{\partial l} = -k_{ext}(\vec{x})L(\vec{x}, \vec{u}) + k_a(\vec{x})L^{eq}(\vec{x}) + k_s(\vec{x}) \int_{4\pi} p(\vec{u}', \vec{u}) d\vec{u}' L(\vec{x}, \vec{u}) \quad (13)$$

The frequency-related subscript  $\nu$  has been removed for simplicity (all quantities are monochromatic); we now introduce an upper-bound value  $\hat{k}_{ext}$  of the extinction coefficient field  $k_{ext}$ . This quantity is uniform over the whole  $\Omega$  domain. Equation 13 can be reformulated as:

$$\frac{\partial L(\vec{x}, \vec{u})}{\partial l} = -\hat{k}_{ext}L(\vec{x}, \vec{u}) + \hat{k}_{ext}S(\vec{x}, \vec{u}) \quad (14)$$

with the following source term:

$$S(\vec{x}, \vec{u}) = L(\vec{x}, \vec{u}) + \frac{1}{\hat{k}_{ext}} \left[ -k_{ext}(\vec{x})L(\vec{x}, \vec{u}) + k_a(\vec{x})L^{eq}(\vec{x}) + k_s(\vec{x}) \int_{4\pi} p(\vec{u}', \vec{u}) d\vec{u}' L(\vec{x}, \vec{u}) \right] \quad (15)$$

If we further assume that  $\hat{k}_{ext}$  is the sum of  $\hat{k}_a$  and  $\hat{k}_s$ , upper-bound values for, respectively, the absorption coefficient field and the scattering coefficient field (these quantities are also uniform among  $\Omega$ ), this source term can be reformulated as:

$$S(\vec{x}, \vec{u}) = \frac{\hat{k}_a}{\hat{k}_{ext}} \left[ \frac{k_a(\vec{x})}{\hat{k}_a} L^{eq}(\vec{x}) + \left(1 - \frac{k_a(\vec{x})}{\hat{k}_a}\right) L(\vec{x}, \vec{u}) \right] + \frac{\hat{k}_s}{\hat{k}_{ext}} \left[ \frac{k_s(\vec{x})}{\hat{k}_s} \int_{4\pi} p(\vec{u}', \vec{u}) d\vec{u}' L(\vec{x}, \vec{u}) + \left(1 - \frac{k_s(\vec{x})}{\hat{k}_s}\right) L(\vec{x}, \vec{u}) \right] \quad (16)$$

Since  $\hat{k}_{ext}$  is uniform in  $\Omega$ , equation 14 has a well known solution:

$$L(\vec{x}, \vec{u}) = L^{\partial\Omega}(\vec{y}, \vec{u}) \exp(-\hat{k}_{ext}l_0) + \int_0^{l_0} \hat{k}_{ext} \exp(-\hat{k}_{ext}l) dl \left\{ S(\vec{x} - l\vec{u}, \vec{u}) \right\} \quad (17)$$

with  $l_0$  the distance between position  $\vec{x}$  and the boundary, in direction  $\vec{u}$ ; first, we can first replace the attenuation term between  $\vec{x}$  and the boundary by  $\int_0^{l_0} \hat{k}_{ext} \exp(-\hat{k}_{ext}l) dl$ ; then we make use of the Heaviside notation:  $\int_0^{l_0} dl = \int_0^{+\infty} \mathcal{H}(\vec{x}' = \vec{x} - l\vec{u} \in \Omega)$ , and  $\int_0^{+\infty} dl = \int_0^{+\infty} \mathcal{H}(\vec{x}' = \vec{x} - l\vec{u} \notin \Omega)$ . The previous solution can then be reformulated under a single integral:

$$L(\vec{x}, \vec{u}) = \int_0^{+\infty} \hat{k}_{ext} \exp(-\hat{k}_{ext}l) dl \left\{ S(\vec{x} - l\vec{u}, \vec{u}) \mathcal{H}(\vec{x}' \in \Omega) + L^{\partial\Omega}(\vec{y}, \vec{u}) \mathcal{H}(\vec{x}' \notin \Omega) \right\} \quad (18)$$

Introducing the source term from relation 16 into this integral form, we obtain:

$$\begin{aligned} L(\vec{x}, \vec{u}) = & \int_0^{+\infty} \hat{k}_{ext} \exp(-\hat{k}_{ext}l) dl \left\{ L^{\partial\Omega}(\vec{y}, \vec{u}) \mathcal{H}(\vec{x}' \notin \Omega) \right. \\ & + \left[ \frac{\hat{k}_a}{\hat{k}_{ext}} \left[ \frac{k_a(\vec{x}')}{\hat{k}_a} L^{eq}(\vec{x}') + \left(1 - \frac{k_a(\vec{x}')}{\hat{k}_a}\right) L(\vec{x}', \vec{u}) \right] \right. \\ & \left. \left. + \frac{\hat{k}_s}{\hat{k}_{ext}} \left[ \frac{k_s(\vec{x}')}{\hat{k}_s} \int_{4\pi} p(\vec{u}', \vec{u}) d\vec{u}' L(\vec{x}', \vec{u}') + \left(1 - \frac{k_s(\vec{x}')}{\hat{k}_s}\right) L(\vec{x}', \vec{u}) \right] \right] \mathcal{H}(\vec{x}' \in \Omega) \right\} \quad (19) \end{aligned}$$

Now, the absorption coefficient at a given frequency  $\nu$  is formalized as the sum of the contributions of  $N_t$  transitions, for the same frequency:  $k_a(\vec{x}) = \sum_{j=1}^{N_t} h_{a,j}$ ; we further introduce an upper-bound  $\hat{h}_{a,j}$  to the contribution of each transition  $j$  to the total absorption coefficient (this upper-bound value is also uniform within  $\Omega$ ), which makes possible to reformulate  $\frac{k_a(\vec{x})}{\hat{k}_a}$  as  $\sum_{j=1}^{N_t} \frac{\hat{h}_{a,j}}{\hat{k}_a} \frac{h_{a,j}(\vec{x})}{\hat{h}_{a,j}}$  and  $1 - \frac{k_a(\vec{x})}{\hat{k}_a}$  can be reformulated as  $\sum_{j=1}^{N_t} \frac{\hat{h}_{a,j}}{\hat{k}_a} \left(1 - \frac{h_{a,j}(\vec{x})}{\hat{h}_{a,j}}\right)$ ; the integral solution now reads:

$$\begin{aligned}
L(\vec{x}, \vec{u}) = & \int_0^{+\infty} \hat{k}_{ext} \exp(-\hat{k}_{ext} l) dl \left\{ L^{\partial\Omega}(\vec{y}, \vec{u}) \mathcal{H}(\vec{x}' \notin \Omega) \right. \\
& + \left[ \frac{\hat{k}_s}{\hat{k}_{ext}} \left[ \frac{k_s(\vec{x}')}{\hat{k}_s} \int_{4\pi} p(\vec{u}', \vec{u}) d\vec{u}' L(\vec{x}', \vec{u}') + \left(1 - \frac{k_s(\vec{x}')}{\hat{k}_s}\right) L(\vec{x}', \vec{u}) \right] \right. \\
& \left. \left. + \frac{\hat{k}_a}{\hat{k}_{ext}} \left[ \sum_{j=1}^{N_t} \frac{\hat{h}_{a,j}}{\hat{k}_a} \left[ \frac{h_{a,j}(\vec{x}')}{\hat{h}_{a,j}} L^{eq}(\vec{x}') + \left(1 - \frac{h_{a,j}(\vec{x}')}{\hat{h}_{a,j}}\right) L(\vec{x}', \vec{u}) \right] \right] \mathcal{H}(\vec{x}' \in \Omega) \right\} \quad (20)
\end{aligned}$$

In terms of the Monte Carlo algorithm associated to this integral formulation, we define the following quantities:

- $\hat{P}_s = \frac{\hat{k}_s}{\hat{k}_{ext}}$  is the probability to retain the “scattering” branch of the algorithm;
- $\frac{\hat{k}_a}{\hat{k}_{ext}}$  is the complementary probability, noted  $1 - \hat{P}_s$ , is the probability to retain the “absorption” branch of the algorithm;
- $P_s(\vec{x}) = \frac{k_s(\vec{x})}{\hat{k}_s}$  is the probability a scattering event is retained. The complementary probability  $1 - \frac{k_s(\vec{x})}{\hat{k}_s}$  is the probability a “null scattering” event is sampled;
- $P_J(j, \nu) = \frac{\hat{h}_{a,j}}{\hat{k}_a}$  is the probability to sample transition of index  $j$  among  $N_t$  transitions, for current frequency  $\nu$ ;
- $P_a(\vec{x}) = \frac{h_{a,j}(\vec{x})}{\hat{h}_{a,j}}$  is the probability a absorption event is sampled, and the complementary probability  $1 - \frac{h_{a,j}(\vec{x})}{\hat{h}_{a,j}}$  is the probability a “null absorption” event is sampled.

With these notations, the integral formulation of the general solution to the radiative transfer equation finally reads:

$$\begin{aligned}
L(\vec{x}, \vec{u}) = & \int_0^{+\infty} \hat{k}_{ext} \exp(-\hat{k}_{ext} l) dl \left\{ L^{\partial\Omega}(\vec{y}, \vec{u}) \mathcal{H}(\vec{x}' \notin \Omega) \right. \\
& + \left[ \hat{P}_s \left[ P_s(\vec{x}) \int_{4\pi} p(\vec{u}', \vec{u}) d\vec{u}' L(\vec{x}', \vec{u}') + \left(1 - P_s(\vec{x})\right) L(\vec{x}', \vec{u}) \right] \right. \\
& \left. \left. + \left(1 - \hat{P}_s\right) \left[ \sum_{j=1}^{N_t} P_J(j, \nu) \left[ P_a(\vec{x}) L^{eq}(\vec{x}') + \left(1 - P_a(\vec{x})\right) L(\vec{x}', \vec{u}) \right] \right] \mathcal{H}(\vec{x}' \in \Omega) \right\} \quad (21)
\end{aligned}$$

that is identical to equation 5.

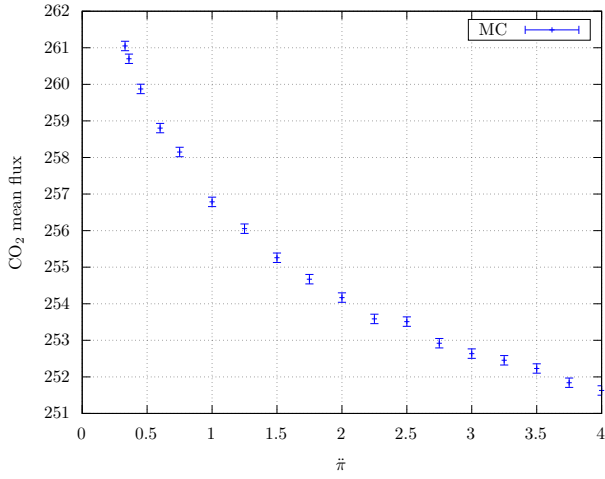
## References

- [1] Pincus, R. et al., "Computational cost and accuracy in calculating three-dimensional radiative transfer : Results for new implementations of monte

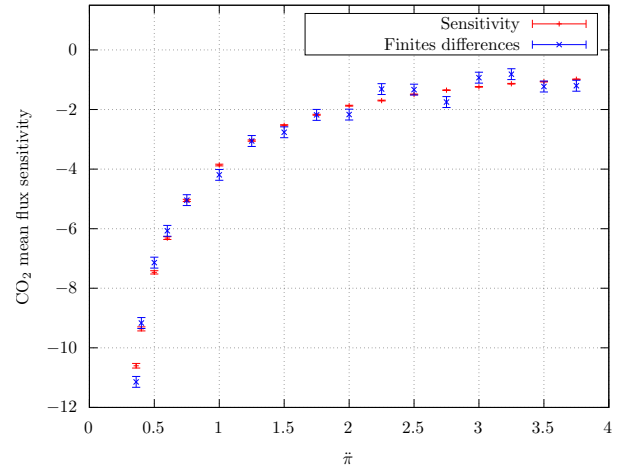
- carlo and SHDOM," *Journal of the Atmospheric Sciences*, 66(10) :3131–3146, 2009.
- [2] Mayer, B., "Radiative transfer in the cloudy atmosphere," *The European Physical Journal Conferences*, 1 :75–99, 2009.
- [3] Niro, F. et al., "European Space Agency (ESA) Calibration/Validation Strategy for Optical Land-Imaging Satellites and Pathway towards Interoperability," *Remote Sensing*, 13(15) :3003, 2021.
- [4] Schwaerzel, M. et al., "Impact of 3d radiative transfer on airborne N O 2 imaging remote sensing over cities with buildings," *Atmospheric Measurement Techniques*, 14(10) :6469–6482, 2021.
- [5] Villefranche, N. et al., "A path-tracing monte carlo library for 3-d radiative transfer in highly resolved cloudy atmospheres," *Journal of Advances in Modeling Earth Systems*, 11(8) :2449–2473, 2019.
- [6] Tregan, J.-M. et al., "Coupling radiative, conductive and convective heat-transfers in a single Monte Carlo algorithm: A general theoretical framework for linear situations," *PLoS ONE*, 18(4): e0283681, 2023.
- [7] Ibarrart, L. et al., "Advection, diffusion and linear transport in a single path-sampling Monte Carlo algorithm : getting insensitive to geometrical refinement," working paper or preprint : <https://hal.science/hal-03818899v2/file/main%20%281%29.pdf>.
- [8] Villefranche, N. et al., "The “teapot in a city” : A paradigm shift in urban climate modeling," *Science Advances*, 8(27), 2022.
- [9] Galtier, M. et al., "Radiative transfer and spectroscopic databases : A line-sampling monte carlo approach," *Journal of Quantitative Spectroscopy and Radiative Transfer*, 172 :83–97, 2016.
- [10] Novák, J. et al., "Monte Carlo methods for volumetric light transport simulation," *Computer Graphics Forum (Proceedings of Eurographics - State of the Art Reports)*, 2018.
- [11] Miller, B. et al., *ACM Transactions on Graphics (Proceedings of SIGGRAPH)*, 2019.
- [12] de Lataillade, A. et al., "Monte carlo method and sensitivity estimations," *Journal of Quantitative Spectroscopy and Radiative Transfer*, 75(5) :529–538., 2002.
- [13] Zeltner, T. et al., "Monte carlo estimators for differential light transport," *ACM Transactions on Graphics*, 40(4) :1–16, 2021.
- [14] El Hafi, M. et al., "Three viewpoints on null-collision monte carlo algorithms," *Journal of Quantitative Spectroscopy and Radiative Transfer*, 260 :107402, 2021.

- [15] Galtier, M. et al., "Integral formulation of null-collision monte carlo algorithms," *Journal of Quantitative Spectroscopy and Radiative Transfer*, 125 :57–68, 2013.
- [16] Nyffenegger-Péré, Y., "Coupler le rayonnement et la spectroscopie raie par raie dans un même algorithme de Monte Carlo : permettre le calcul de référence des forçages radiatifs", PhD thesis, Paul Sabatier University *submitted for publication*.
- [17] Tregan, J.-M. et al., "Convergence issues in derivatives of monte carlo null-collision integral formulations : A solution," *Journal of Computational Physics*, 413:109463, 2020.
- [18] Lapeyre, P. et al., "Monte carlo and sensitivity transport models for domain deformation," *Journal of Quantitative Spectroscopy and Radiative Transfer*, 251 :107022, 2020.
- [19] Lapeyre, P. et al., "A physical model and a monte carlo estimate for the specific intensity spatial derivative, angular derivative and geometric sensitivity," working paper or preprint : <https://arxiv.org/abs/2206.05167>.
- [20] Gordon, Iouli E., et al. "The HITRAN2020 molecular spectroscopic database." *Journal of quantitative spectroscopy and radiative transfer* , 277:107949, 2022.
- [21] Boucher, Olivier, et al. "Presentation and evaluation of the IPSL-CM6A-LR climate model." *Journal of Advances in Modeling Earth Systems*, 12.7:e2019MS002010, 2020.
- [22] Pincus, R. et al., "Benchmark Calculations of Radiative Forcing by Greenhouse Gases," *Journal of Geophysical Research: Atmospheres*, 125, 23:e2020JD033483, 2020.
- [23] Ogura, T. et al., "Importance of instantaneous radiative forcing for rapid tropospheric adjustment," *Climate Dynamics*, 43, 2013.
- [24] IPCC, *Climate Change: The IPCC Scientific Assessment*, Pages 365, Published by Cambridge University Press, Year 1980, Editors: Houghton, J. T., Jenkins, G.J., Ephraums, J.J.
- [25] Jeevanjee, N. et al., "An Analytical Model for Spatially Varying Clear-Sky CO<sub>2</sub> Forcing," *Journal of Climate (J. Clim.)*, Volume 34, Number 23, 2021.
- [26] McCool, M.D. et al., "Probability trees," *Proceedings of the conference on Graphics interface*, 1997.
- [27] Maire, S. et al., "Stochastic finite differences for elliptic diffusion equations in stratified domains," *Mathematics and Computers in Simulation*, 121:146–165, 2016.
- [28] Bossy, M. et al., "Monte Carlo methods for linear and non-linear Poisson-Boltzmann equation," *ESAIM: Proceedings and Surveys*, 48:420–446, 2015.

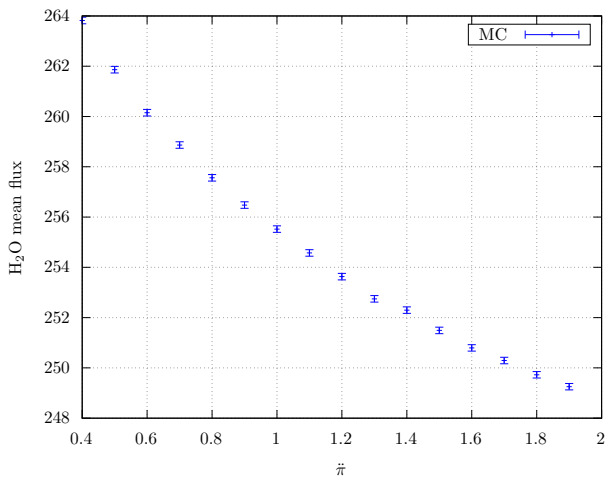
- [29] Farges, O. et al., "Life-time integration using Monte Carlo Methods when optimizing the design of concentrated solar power plants", *Solar Energy*, 113, 2015.
- [30] Terrée, G. et al., "Addressing the Gas Kinetics Boltzmann Equation with Branching-Path Statistics," *Physical Review E*, 105(2):025305, 2022.



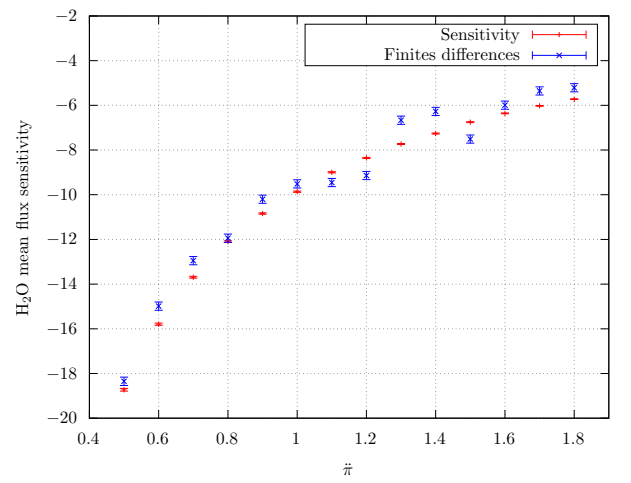
(a) Variation of  $\bar{\phi}$  as a function of fraction change in  $x_{CO_2}$ .



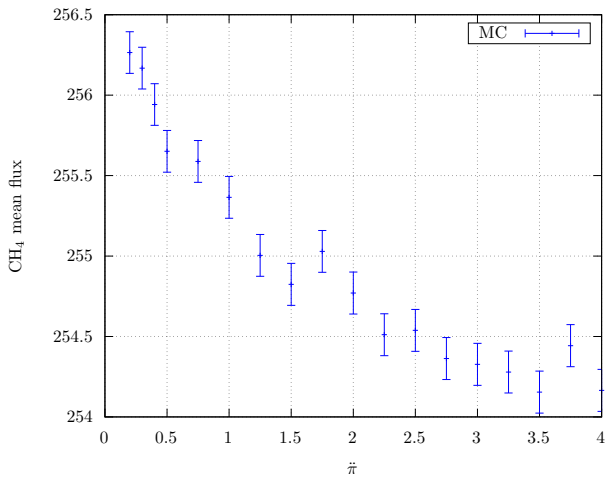
(b) Variation of  $\partial_{\bar{\pi}}\bar{\phi}$  as a function of fraction change in  $x_{CO_2}$ .



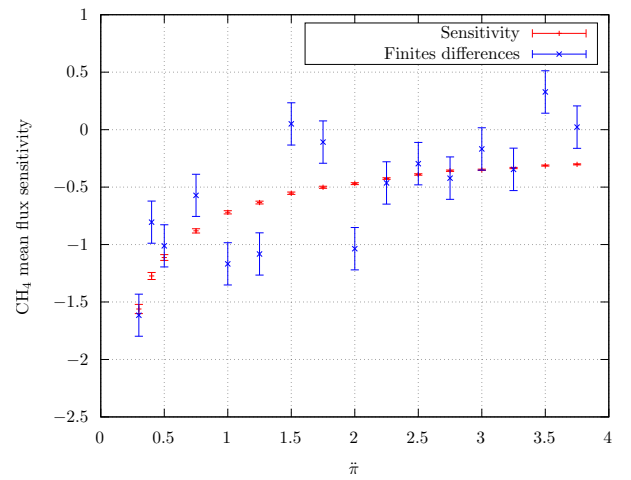
(c) Variation of  $\bar{\phi}$  as a function of fraction change in  $x_{H_2O}$ .



(d) Variation of  $\partial_{\bar{\pi}}\bar{\phi}$  as a function of fraction change in  $x_{H_2O}$ .



(e) Variation of  $\bar{\phi}$  as a function of fraction change in  $x_{CH_4}$ .



(f) Variation of  $\partial_{\bar{\pi}}\bar{\phi}$  as a function of fraction change in  $x_{CH_4}$ .

Figure 3: Mean flux and sensitivities associated to a change in the fraction of gas concentration  $\bar{\pi}$  are displayed for three gases:  $CO_2$  (Fig. 3a and Fig. 3b),  $H_2O$  (Fig. 3c and Fig. 3d), and  $CH_4$  (Fig. 3e and Fig. 3f). Sensitivity estimates are obtained using Algorithm 2, whereas finite difference estimates are based on the difference between two standard Monte Carlo flux estimates obtained for different values of  $\bar{\pi}$  using Algorithm 1. Error bars: 68% CI (using  $1\sigma$ ).

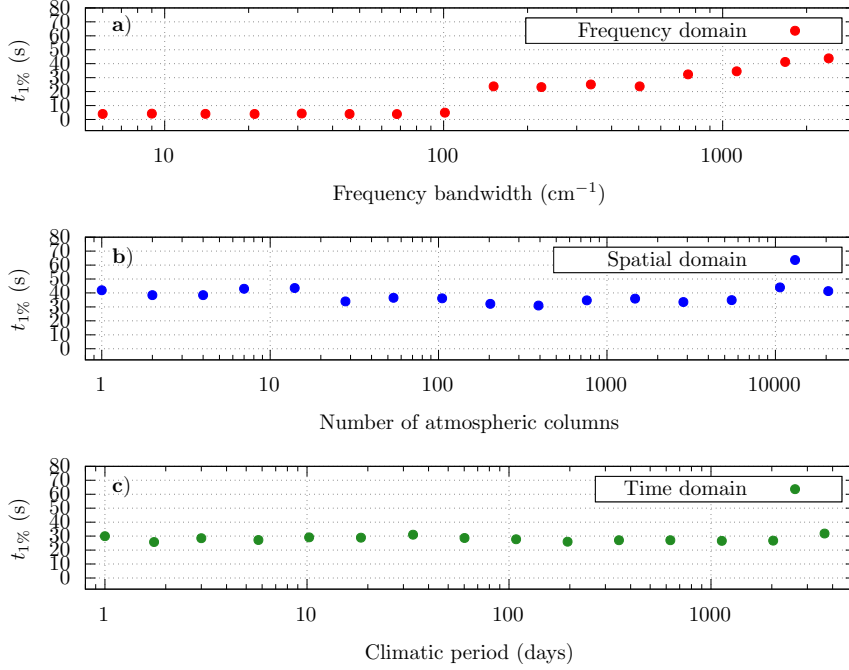


Figure 4: Computation time required to estimate sensitivity of an outgoing radiative flux with respect to fraction change in  $\text{CO}_2$  concentration field, estimated at a 1% relative error using  $1\sigma$ , showing only a slight dependency to the frequency bandwidth (first plot), spatial (second plot) and temporal (third plot) domains widening.

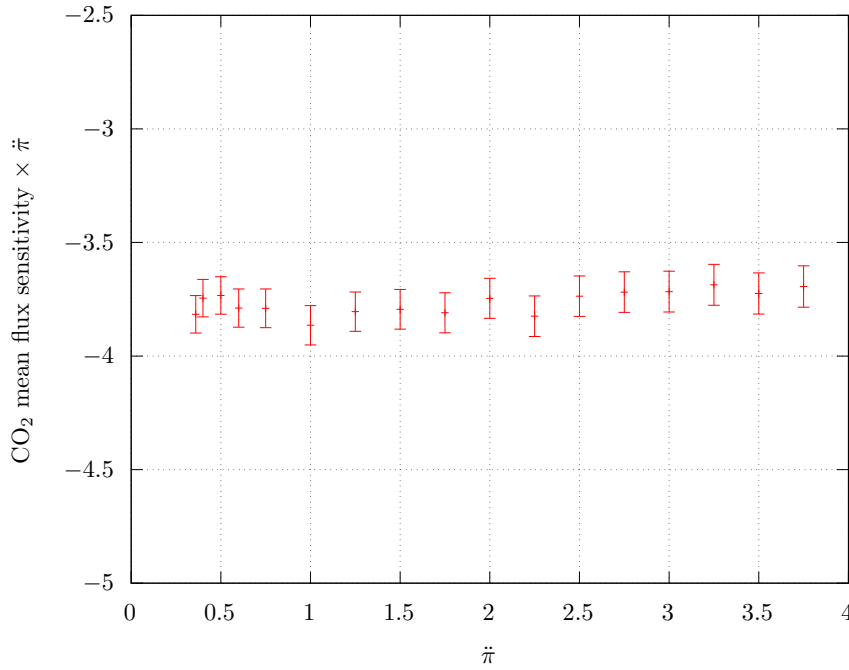


Figure 5: Evolution of  $\partial_{\bar{\pi}} \bar{\phi}$  ( $\text{CO}_2$  sensitivity) multiplied by parameter  $\bar{\pi}$  as a function of  $\bar{\pi}$ . Error bars: 99% CI (using  $3\sigma$ ).